SiO_2 etch characteristics and environmental impact of Ar/C_3F_6O chemistry

Ho Seok Lee, Kyung Chae Yang, Soo Gang Kim, Ye Ji Shin, Dae Woong Suh, Han Dock Song, Nae Eung Lee, and Geun Young Yeom

Citation: Journal of Vacuum Science & Technology A **36**, 061306 (2018); doi: 10.1116/1.5027446
View online: https://doi.org/10.1116/1.5027446
View Table of Contents: http://avs.scitation.org/toc/jva/36/6
Published by the American Vacuum Society

SiO_2 etch characteristics and environmental impact of Ar/C_3F_6O chemistry

Ho Seok Lee,[1] Kyung Chae Yang,[2] Soo Gang Kim,[1] Ye Ji Shin,[2] Dae Woong Suh,[3] Han Dock Song,[3] Nae Eung Lee,[1,2] and Geun Young Yeom[1,2,a)]
[1]*SKKU Advanced Institute of Nano Technology (SAINT), Sungkyunkwan University, Suwon, Gyeonggi-Do 16419, Republic of Korea*
[2]*School of Advanced Materials Science and Engineering, Sungkyunkwan University, Suwon, Gyeonggi-Do 16419, Republic of Korea*
[3]*Wonik Materials Co., Ltd., Research and Development Group, Cheongju 28215, Republic of Korea*

(Received 2 March 2018; accepted 19 October 2018; published 20 November 2018)

Perfluorocarbon gases are commonly used for nanoscale etching in semiconductor processing; however, they have the disadvantages of a long lifetime and inducing global warming effects when released into the atmosphere. In this study, the SiO_2 etch characteristics and global warming effects of C_3F_6O gas chemistry, which has a low global warming potential, were compared with those of C_4F_8 chemistry, which is commonly used in semiconductor processing. Using Ar/C_3F_6O, the SiO_2 etch rate was higher and the etch selectivity of SiO_2 over the amorphous carbon hardmask layer was lower than the etch rate and etch selectivity using $Ar/C_4F_8/O_2$, with all other etch conditions the same. Furthermore, using Ar/C_3F_6O exhibited more anisotropic SiO_2 etch profiles by suppressing the bowing, narrowing, and necking effects compared to the etch profiles using $Ar/C_4F_8/O_2$. The global warming effects were evaluated by calculating the million metric ton carbon equivalents (MMTCEs) from the volumetric concentrations of the emitted by-product species and process gases, and the results showed that, in the optimized conditions, Ar/C_3F_6O exhibited a lower environmental impact with an MMTCE of <24% than that of $Ar/C_4F_8/O_2$. Therefore, it is suggested that the Ar/C_3F_6O gas mixture is a potential replacement for $Ar/C_4F_8/O_2$ because of its lower MMTCE and acceptable SiO_2 etch characteristics. *Published by the AVS.* https://doi.org/10.1116/1.5027446

I. INTRODUCTION

In semiconductor manufacturing, as device size reduces to the scale of tens of nanometers for better performance and for ultra-large-scale integration, high-aspect-ratio contacts (HARCs) with highly anisotropic etch profiles become an essential part of semiconductor devices such as dynamic random-access memory and 3D NAND.[1–5] However, the difficulty level of the manufacturing process has drastically increased with the growing degree of integration, and controlling the critical dimension while simultaneously lowering the plasma-induced damage has become critical.[6–8] For HARC etching, in particular, it is imperative to solve profile distortion problems such as sidewall bowing, bottom distortion, and the notching effect[9–12] to obtain an acceptable etch profile.

Perfluorocarbons (PFCs) such as CF_4, C_2F_6, C_3F_8, and C_4F_8 are used in the etching of dielectrics such as silicon dioxide (SiO_2) and silicon nitride (Si_3N_4) because these chemistries exhibit the desired etch selectivities over silicon or mask layers [i.e., amorphous carbon layers (ACLs) and photoresist] by forming upon them a fluorocarbon polymer of sufficient thickness for selective etching.[13–20] Unfortunately, these PFCs are strong global warming gases possessing long atmospheric lifetimes and high global warming potential (GWP) values. Hence, they have significant negative effects on the environment by strongly absorbing infrared radiation.[21–23]

As the Paris agreement goes into effect in 2020 followed by the Kyoto protocol commitment, reducing emissions and the use of PFC gases is emerging as a serious issue in the semiconductor and display industries.[24–26] Therefore, in recent years, there has been an increase in research efforts to reduce the emission of PFCs in semiconductor processing by substituting high-GWP PFCs with low-GWP gases or by using PFC gases with high boiling points such as liquid fluorocarbon, where the latter is recoverable as a liquid at the exhaust line after use, that can provide satisfactory levels of performance.[27–31] For example, attempts to replace high-GWP fluorocarbon gases with low-GWP gases such as C_3F_6, C_5F_8, and C_4F_6 have been made.[32–36] Among them, C_4F_6 is currently used in some contact dielectric etching processes as a replacement for C_4F_8 because it exhibits good etch characteristics. However, a large amount of C_4F_8 mixed with Ar/O_2 is still used in dielectric etching in addition to C_4F_6 to control the etch profile or to maintain a certain C/F ratio. Therefore, it is necessary to investigate other alternative low-GWP PFC gases to replace C_4F_8.

Oxygen-containing fluorocarbon gases such as C_4F_8/O_2 and C_3F_6O have been investigated as low-GWP chamber cleaning gases for the chemical vapor deposition (CVD) of Si_3N_4 or SiO_2, replacing high-GWP chamber cleaning gases such as SF_6 and NF_3.[13,31,33,37] Recent studies on C_3F_6O have shown that C_3F_6O/O_2 can be used to remove Si_3N_4 and SiO_2 deposited on the CVD chamber in place of SF_6 or NF_3.[13,31] In fact, for dielectric etching using C_4F_8, a gas mixture composed of $Ar/C_4F_8/O_2$ is generally used rather than C_4F_8 alone. Therefore, in this study, the etch characteristics such as

a)Electronic mail: gyyeom@skku.edu

etch rate and etch selectivity of contact dielectric etching were investigated using C_3F_6O, to determine its eligibility as a contact dielectric etchant gas to replace the C_4F_8/O_2 gas mixture. The C_3F_6O has a very short lifetime (<1 year) and an extremely low GWP_{100} (<100) compared to C_4F_8 (lifetime of 3200 years and GWP_{100} of 10 300), as shown in Table I. Therefore, C_3F_6O, which easily decomposes in the atmosphere, can reduce the impact on the environment and the environmental costs during both the plasma-on times and the plasma-off times used to stabilize the process during dielectric etching. To confirm the environmental effects of the Ar/C_3F_6O chemistry quantitatively, its million metric ton carbon equivalent (MMTCE) values were estimated using the concentrations of the by-product species in the exhaust gas and by the GWPs of the by-product species. The results showed that Ar/C_3F_6O is a potential replacement gas mixture for $Ar/C_4F_8/O_2$, because of its low MMTCE and its acceptable capability of selective etching of SiO_2 over a mask layer.

II. EXPERIMENT

In this study, a home-made dual-frequency capacitively-coupled plasma (DF-CCP) system was used. The chamber and the bottom/top electrodes were of anodized aluminum. Each electrode was 200 mm in diameter, and the outer side of each electrode was supported by a ceramic ring for insulation. The top electrode was perforated to inject reactive gases into the vacuum chamber uniformly over the wafer surface, and the two electrodes were separated in parallel by a distance of 80 mm. An rf power of 60 MHz was supplied to the top electrode to control the plasma characteristics such as ion densities, radical densities, and their fluxes to the substrate, while 2 MHz rf power was supplied to the bottom electrode to control the ion bombardment energy on the substrate. The chamber was evacuated using a turbo molecular pump (EBARA 1606W-TF) backed by a dry pump (Alcatel ADP 122P), and the process pressure was automatically maintained by adjusting a throttle valve during etching.

A 2 μm-thick SiO_2 layer was deposited on an Si wafer and was subsequently masked with an ACL possessing hole patterns 100 nm in diameter and 600 nm in thickness, which was used as the hardmask for SiO_2 contact etching. Next, 150/50 sccm of Ar/C_3F_6O (HFPO, hexafluoropropylene oxide) gas mixture and 150/50/10 sccm of Ar/c-C_4F_8 (perfluorocyclobutane, PFC-318)/O_2 gas mixture were used while varying the power of the source and bias. The operating pressure and substrate temperature were maintained at 30 mTorr and room temperature, respectively.

The plasma characteristics during etching with the Ar/C_3F_6O and $Ar/C_4F_8/O_2$ gas mixtures were investigated by optical emission spectroscopy (OES, Andor iStar 734). The etch characteristics such as the etch rates and etch profiles of SiO_2 and the ACL were estimated by field-emission scanning electron microscopy (Hitachi S-4700) using the ACL-patterned SiO_2 wafers. For optimized etch conditions, any ACL that remained on the SiO_2 hole pattern after etching was removed with an inductively coupled plasma system to enable observation of the etched SiO_2 hole pattern. For this, a 13.56 MHz rf source power of 300 W and a separate 13.56 MHz rf bias power of −50 V and 100 sccm O_2 were used, where the operating pressure was maintained at 20 mTorr. The process time was 6 min. In addition, the surface chemistries of the etched SiO_2 blanket unit thin films for Ar/C_3F_6O and $Ar/C_4F_8/O_2$ were observed using x-ray photoelectron spectroscopy (XPS, VG Microtech Inc., ESCA 2000) to investigate the carbon binding states of fluorocarbon polymer layers remaining on the etched SiO_2 surfaces.

The volumetric concentrations of the by-product PFC species and parent PFC gases were measured using a Fourier-transform infrared (FT-IR, MIDAC I2000) spectroscopy system, which was connected to the exhaust line backed by a rotary pump, as shown in Fig. 1. The MMTCEs were calculated using

$$\mathrm{MMTCE} = \sum_i \frac{12}{44} \times \frac{\mathrm{M}_i(\mathrm{kg}) \times GWP_{100i}}{10^9}, \tag{1}$$

where GWP_{100i} is the global warming potential integrated over a 100-year time horizon and M_i is the total weight of the emitted PFCs, as measured by FT-IR during the process. The values of GWP_{100i} used in the calculation are given in Table I. The effects of Ar/C_3F_6O and $Ar/C_4F_8/O_2$ on global warming during etching were quantified via the MMTCEs.

TABLE I. Atmospheric lifetimes and GWP of various gases.

Acronym, chemical name	Chemical formula	Atmospheric lifetime (years)	GWP_{100}	References
Carbon dioxide	CO_2	50–200	1	34, 35
Carbon monoxide	CO	50–200	3	31
Carbonyl Fluoride	COF_2	50–200	1	31
Carbon tetrafluoride (PFC-14)	CF_4	50 000	6500	34, 35
Perfluorocyclobutane (PFC-318)	c-C_4F_8	3200	8700	34, 35
Hexafluoroethane (PFC-116)	C_2F_6	10 000	9200	34, 35
Octafluoropropane	C_3F_8	2600	7000	34, 35
Hexafluoropropylene oxide	C_3F_6O	<1	<100	13, 28

III. RESULTS AND DISCUSSION

The SiO_2 masked with ACL was etched with Ar/C_3F_6O and $Ar/C_4F_8/O_2$ using the DF-CCP system. The etch rates of

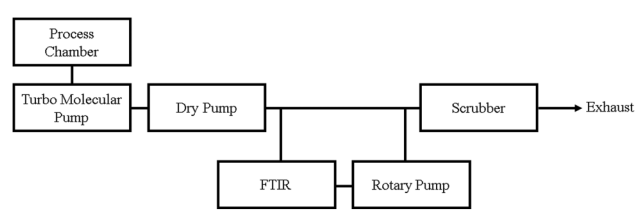

FIG. 1. Schematic of the gas sampling structure of the DF-CCP etch system herein.

the SiO_2 and ACL and the etch selectivity of SiO_2 over the ACL were measured, and the results are shown in Fig. 2. The etch rates of SiO_2 and the ACL were also estimated after etching to a ~1 μm depth of the SiO_2 contact hole. For this, 100–400 W of 60 MHz rf power for the source and −800 to −1700 V of 2 MHz rf power for the substrate biasing were used, while maintaining 30 mTorr operating pressure for both Ar/C_3F_6O (150/50 sccm) and $Ar/C_4F_8/O_2$ (150/50/10 sccm). The optimized $Ar/C_4F_8/O_2$ gas composition reported in a previous study[20] was used for $Ar/C_4F_8/O_2$ in this experiment. Figures 2(a) and 2(b) show the etch rates and etch selectivity of SiO_2 and the ACL measured as functions of the source power and bias power, respectively, for Ar/C_3F_6O. In Fig. 2(a), when the 60 MHz rf power was varied, the 2 MHz rf bias voltage was maintained at −1100 V; and in Fig. 2(b), when the 2 MHz rf power was varied, the 60 MHz rf source power was maintained at 200 W. To etch to a depth of ~1 μm in SiO_2 when using C_3F_6O, the process time of Fig. 2(a) was varied as 10 min, 4 min 40 s, 3 min, and 2 min 30 s for 100, 200, 300, and 400 W, respectively. The process time in Fig. 2(b) was varied as 7 min, 4 min 40 s, 3 min 30 s, and 3 min when the conditions were −800, −1100, −1400, and −1700 V, respectively. As shown, the increase in the rf source power from 100 to 400 W [Fig. 2(a)] and bias power from −800 to −1700 V [Fig. 2(b)] increased the etch rates of SiO_2 from 100 to 400 nm/min and from 143 to 333 nm/min, respectively. Even though the etch selectivity of SiO_2/ACL did not vary significantly, the increase in the rf source power beyond 200 W decreased the etch selectivity from 3 to 2.7. This decreased SiO_2 etch selectivity is related to the increased etch rate of the ACL caused by the higher concentration of the F radical resulting from the increased dissociation of C_3F_6O. However, an increase in the rf bias power increased the etch selectivity continuously from 2.5 to 3.2, which is attributed to the difference in the fluorocarbon layer formed on the SiO_2 surface and on the ACL. Therefore, the etch rate of SiO_2 is higher, as compared to that of the ACL, with increasing bias voltage.[38,39]

Figures 2(c) and 2(d) show the etch rates and etch selectivity of SiO_2 and the ACL measured as functions of the source power (at −1100 V of bias voltage) and bias power (at 200 W of rf source power), respectively, for the $Ar/C_4F_8/O_2$ chemistry. To etch to a depth of ~1 μm in SiO_2, the process times in Fig. 2(c) were varied as 8 min 10 s, 7 min 40 s, 6 min, and 4 min 20 s for 100, 200, 300, and 400 W, respectively; and the process times in Fig. 2(d) were varied as 9 min 20 s, 7 min 40 s, 5 min 30 s, and 4 min for −800, −1100, −1400, and −1700 V, respectively. Similar to the Ar/C_3F_6O chemistry in Figs. 2(a) and 2(b), the increase in the rf source power and bias voltage increased the SiO_2 etch rates. The SiO_2 etch selectivity over the ACL decreased with an increase in the rf source power and slightly increased with

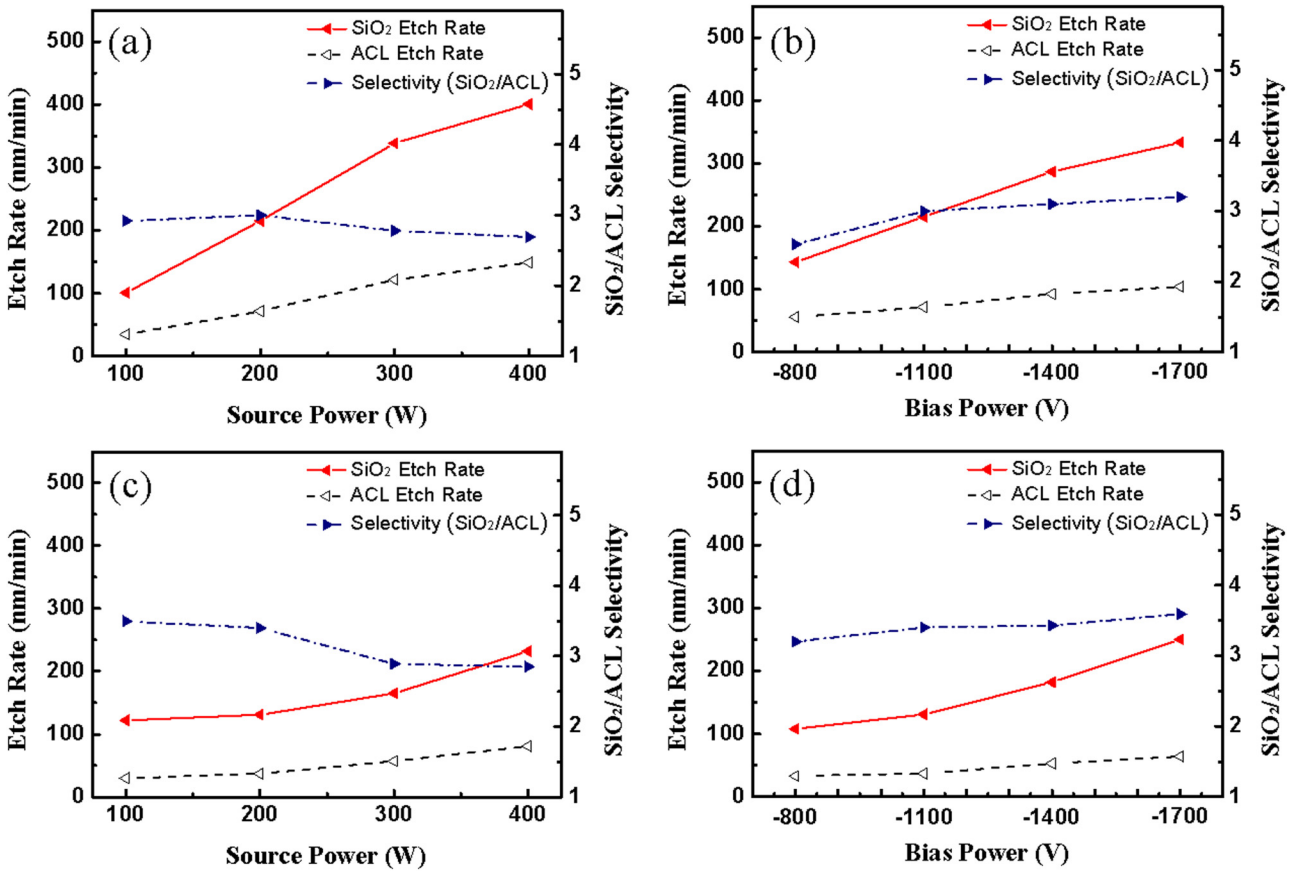

FIG. 2. Etch rates of SiO_2 and ACL and their etch selectivities measured as functions of [(a) and (c)] the source power (at −1100 V of bias voltage using 2 MHz rf bias power) and [(b) and (d)] the bias power (at 200 W of 60 MHz rf source power), respectively, for [(a) and (b)] Ar/C_3F_6O chemistry and [(c) and (d)] $Ar/C_4F_8/O_2$ chemistry. Ar/C_3F_6O = 150/50 sccm, $Ar/C_4F_8/O_2$ = 150/50/10 sccm and an operating pressure of 30 mTorr were used.

rf bias power, similar to the case of Ar/C_3F_6O. However, the SiO_2 etch rates were lower and the SiO_2 etch selectivities over the ACL were slightly higher for the $Ar/C_4F_8/O_2$ chemistry compared to the Ar/C_3F_6O chemistry, when using similar conditions.

Figures 3(a)–3(h) show the variation of rf source power while maintaining the rf bias voltage at −1100 V for the $Ar/C_3F_6/O_2$ and $Ar/C_4F_8/O_2$ chemistries, respectively. Owing to the increased dissociation of C_3F_6O and C_4F_8, the etch profiles were not vertical when the rf source power was greater than 200 W (not shown). Therefore, 200 W was set as the limit of the rf source power and the SiO_2 etch depth was maintained at about 1 μm by controlling the etch time. As shown in Fig. 3, the increase in the rf bias voltage from −800 to −1700 V improved the etch profile of SiO_2 by exhibiting less necking, bowing, narrowing, and tilting, which is possibly owing to the increase in the etch rate and etch selectivity with the increase in rf bias power and owing to increased ion energy at the bottom of the etched SiO_2 trench. The SiO_2 etch profiles of Ar/C_3F_6O were more anisotropic compared to those of Ar/C_4F_8 for the same rf bias power conditions, as shown in Fig. 3. In particular, when the rf bias voltage was −1700 V, the etch profile for the Ar/C_3F_6O was the most anisotropic among the conditions investigated.

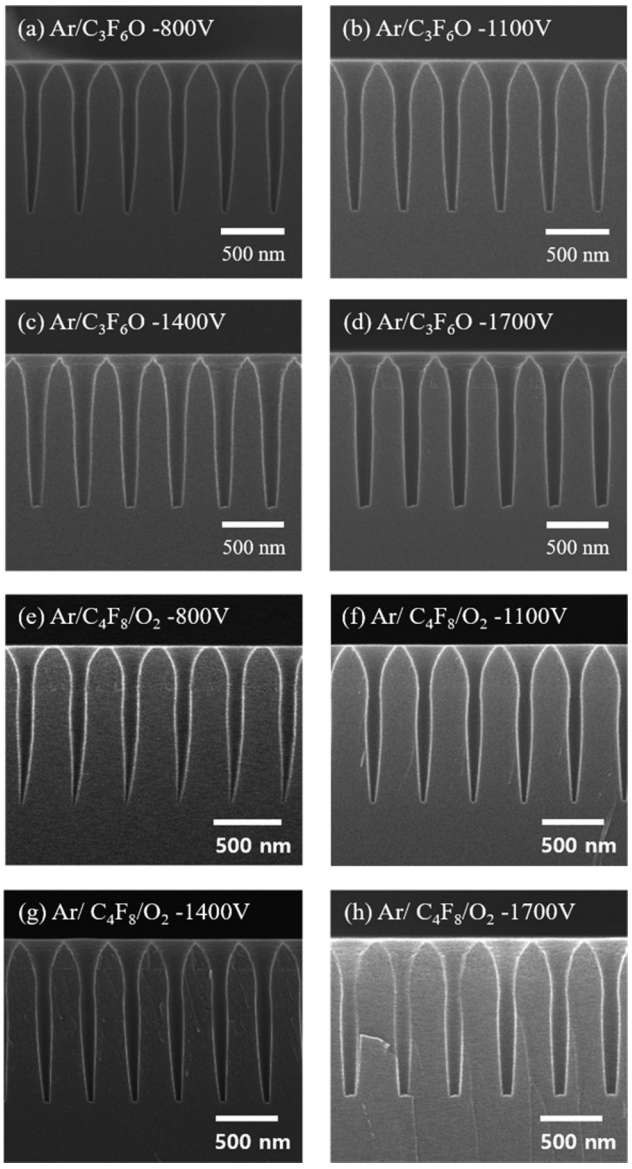

FIG. 3. Etch profiles of SiO_2 masked with ACL for [(a)–(d)] Ar/C_3F_6O and [(e)–(h)] $Ar/C_4F_8/O_2$ for the different rf bias power conditions given in Figs. 2(b) and 2(d). [(a) and (e)] −800 V, [(b) and (f)] −1100 V, [(c) and (g)] −1400 V, and [(d) and (h)] −1700V. The etch time was controlled to obtain an SiO_2 etch depth of 1 μm.

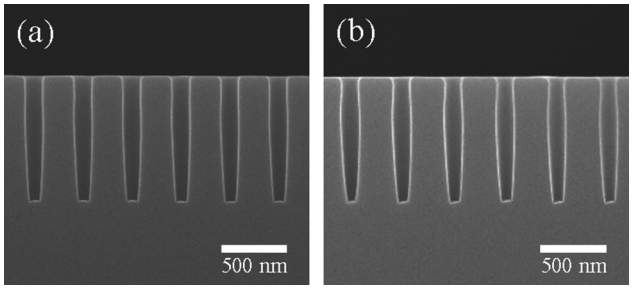

FIG. 4. Etch profiles of only SiO_2 for the conditions of (a) Ar/C_3F_6O and (b) $Ar/C_4F_8/O_2$ in Figs. 3(d) and 3(h) after removing the ACL layer on the etched SiO_2 via O_2 plasma.

Using the conditions of Ar/C_3F_6O and $Ar/C_4F_8/O_2$ given in Figs. 3(d) and 3(h), the ACL layer on the etched SiO_2 was removed and the etch profiles of the SiO_2 hole were compared, where the results are shown in Figs. 4(a) and 4(b) for Ar/C_3F_6O and $Ar/C_4F_8/O_2$, respectively. The ACL layer was removed using O_2 plasma, as described in Sec. II. The SiO_2 profile etched with Ar/C_3F_6O was highly anisotropic, while that etched with $Ar/C_4F_8/O_2$ was slightly less anisotropic and exhibited necking and bowing. Therefore, it is deduced that using Ar/C_3F_6O results in comparable SiO_2 etch characteristics as those using $Ar/C_4F_8/O_2$, even though the etch selectivity of SiO_2 over ACL mask with Ar/C_3F_6O is not as high as in the case of $Ar/C_4F_8/O_2$.

Figures 5(a) and 5(b) show the OES data obtained during etching using Ar/C_3F_6O and $Ar/C_4F_8/O_2$ for the respective

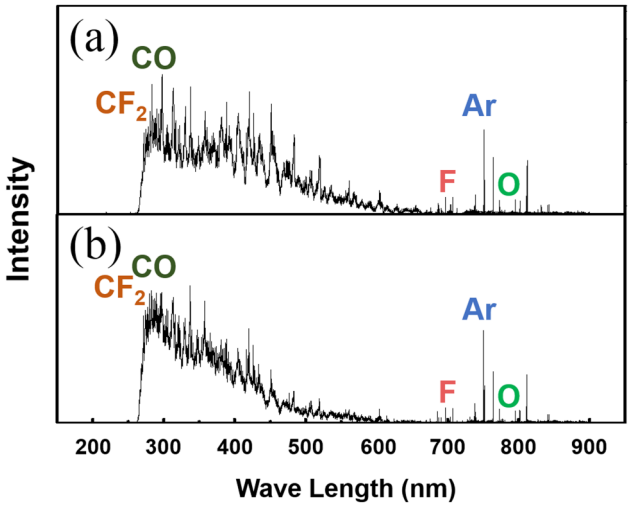

FIG. 5. OES data obtained during etching with (a) Ar/C_3F_6O and (b) $Ar/C_4F_8/O_2$ for the respective optimized etch conditions in Figs. 4(a) and 4(b).

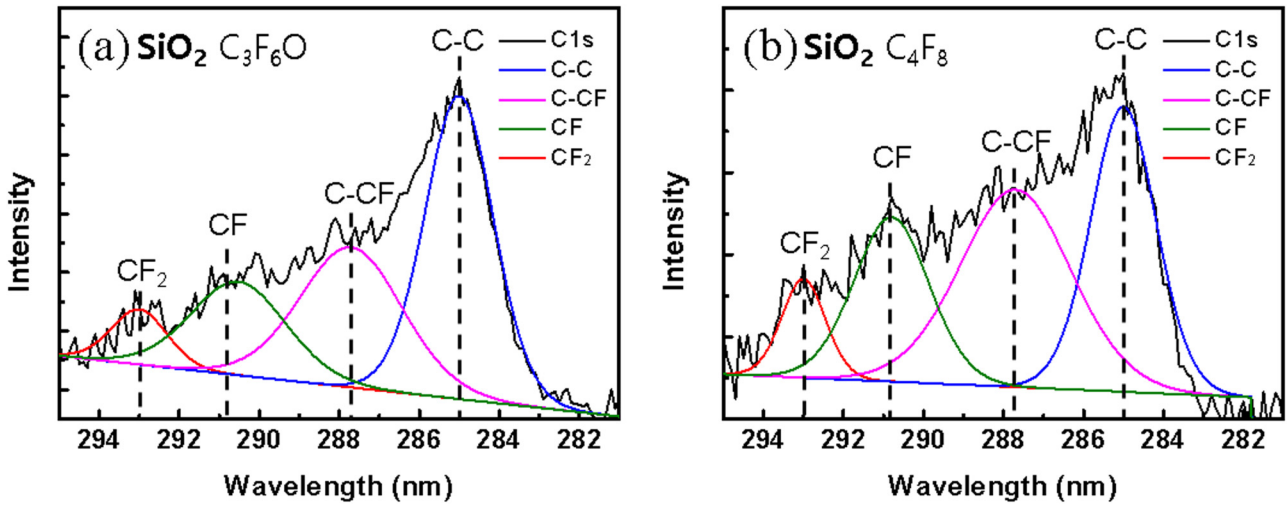

FIG. 6. XPS spectra of C1s narrow scan data on blanket unit thin film SiO_2 after etching using (a) Ar/C_3F_6O and (b) $Ar/C_4F_8/O_2$ for the optimized etch conditions in Fig. 4(a) for Ar/C_3F_6O and Fig. 4(b) for $Ar/C_4F_8/O_2$.

optimized etch conditions in Figs. 4(a) and 4(b). As shown in Figs. 5(a) and 5(b), the optical emission peaks attributed to CF_2 (270–320 nm), CO (283–520 nm), O (437–544 nm), F (701 and 704 nm), Ar (750 nm), and O (777, 785, and 844 nm) could be identified. Furthermore, the peaks attributed CO and O were higher for Ar/C_3F_6O while those attributed to CF_2 were higher for $Ar/C_4F_8/O_2$. Therefore, the higher SiO_2 etch rate and lower SiO_2 etch selectivity over the ACL for the Ar/C_3F_6O chemistry are related to less CF_2 in the plasma, which is owing to the higher dissociation of C_3F_6O compared to that of C_4F_8.

Next, the fluorocarbon polymer layer remaining on the SiO_2 surface during etching using Ar/C_3F_6O and $Ar/C_4F_8/O_2$ was examined using XPS. Figures 6(a) and 6(b) show the C1s narrow scan data measured from SiO_2 during the etching using the conditions in Fig. 4(a) for Ar/C_3F_6O and Fig. 4(b) for $Ar/C_4F_8/O_2$. As shown in Fig. 6, the carbon binding peaks related to C–C (285.0 eV), C–CF (287.7 eV), C–F (290.5 eV), and C–F_2 (292.5 eV) were observed. The peak energies were calibrated using the C1 peak at 285.0 eV. The composition of the fluorocarbon layers on the SiO_2 surface was also measured for $Ar/C_4F_8/O_2$ and Ar/C_3F_6O, and the results are shown in Table II. After the sputter etching, the relative atomic percentages of the material surfaces exhibited a decrease of C and F percentages while those of O and Si were increased. Also, as shown in Table II, the $Ar/C_4F_8/O_2$ exhibited higher percentages of C and F than Ar/C_3F_6O, while the silicon percentage was lower for $Ar/C_4F_8/O_2$ than for Ar/C_3F_6O, which possibly indicates a thicker fluorocarbon layer on the SiO_2 surface etched with $Ar/C_4F_8/O_2$. Therefore, the increased anisotropy of the etch profile for Ar/C_3F_6O compared to that for $Ar/C_4F_8/O_2$ for the respective optimized conditions given in Figs. 4(a) and 4(b) is inferred to be related to the formation of a thinner sidewall fluorocarbon polymer layer on the etched SiO_2 and a lower $CF_x(x = 1, 2)/F$ in the plasma.

The volumetric concentration of the chemical species emitted after SiO_2 etching by the recombination of the dissociated and etched species and the residual feed gas species were measured for Ar/C_3F_6O and $Ar/C_4F_8/O_2$ using FT-IR located at the exhaust line between the dry pump and the scrubber, as schematically shown in Fig. 1. Figure 7 shows the emitted chemical species observed by FT-IR during the etching of SiO_2 using Ar/C_3F_6O as a function of rf source power varying as 100, 200, 300, and 400 W [Fig. 2(a)]. The FT-IR measurements were carried out before the plasma-on for 1 min, during the plasma-on for 2 min, and after the plasma-on for 1 min. In addition to C_3F_6O, the emitted species COF_2, CF_4, C_2F_6, CO, and SiF_4 were observed and their concentration was measured as a function of time (Fig. 7). Herein, CO_2 was also observed at concentrations lesser than that of COF_2 and, owing to significant fluctuation with pressure, these data were not included in Fig. 7. As shown in Figs. 7(a)–7(d), immediately following plasma-on, the concentration of C_3F_6O decreased significantly owing to the plasma-induced dissociation of C_3F_6O, and the concentration of dissociated/recombined species such as COF_2, C_2F_6, CF_4, and CO increased. With an increase in the rf source power from 100 to 200 W, the concentration of C_3F_6O decreased and, for rf source power equal to and higher than 200 W, the C_3F_6O was completely dissociated. During the duration of plasma-on, an increasing rf source power increased the concentrations of CF_4 and C_2F_6, (originating from the recombined radicals of C_3F_6O), of CO

TABLE II. Composition of the SiO_2 surface etched using $Ar/C_4F_8/O_2$ and Ar/C_3F_6O.

		Composition (%)			
Etch gas		C1s	F1s	O1s	Si2p
Ar/C_3F_6O	As-is	5.9	4.8	58.2	31
	After 60 s sputter	3.8	2	61.2	33
$Ar/C_4F_8/O_2$	As-is	4.9	7.6	58.1	29.4
	After 60 s sputter	4.5	3.1	60.3	32.1

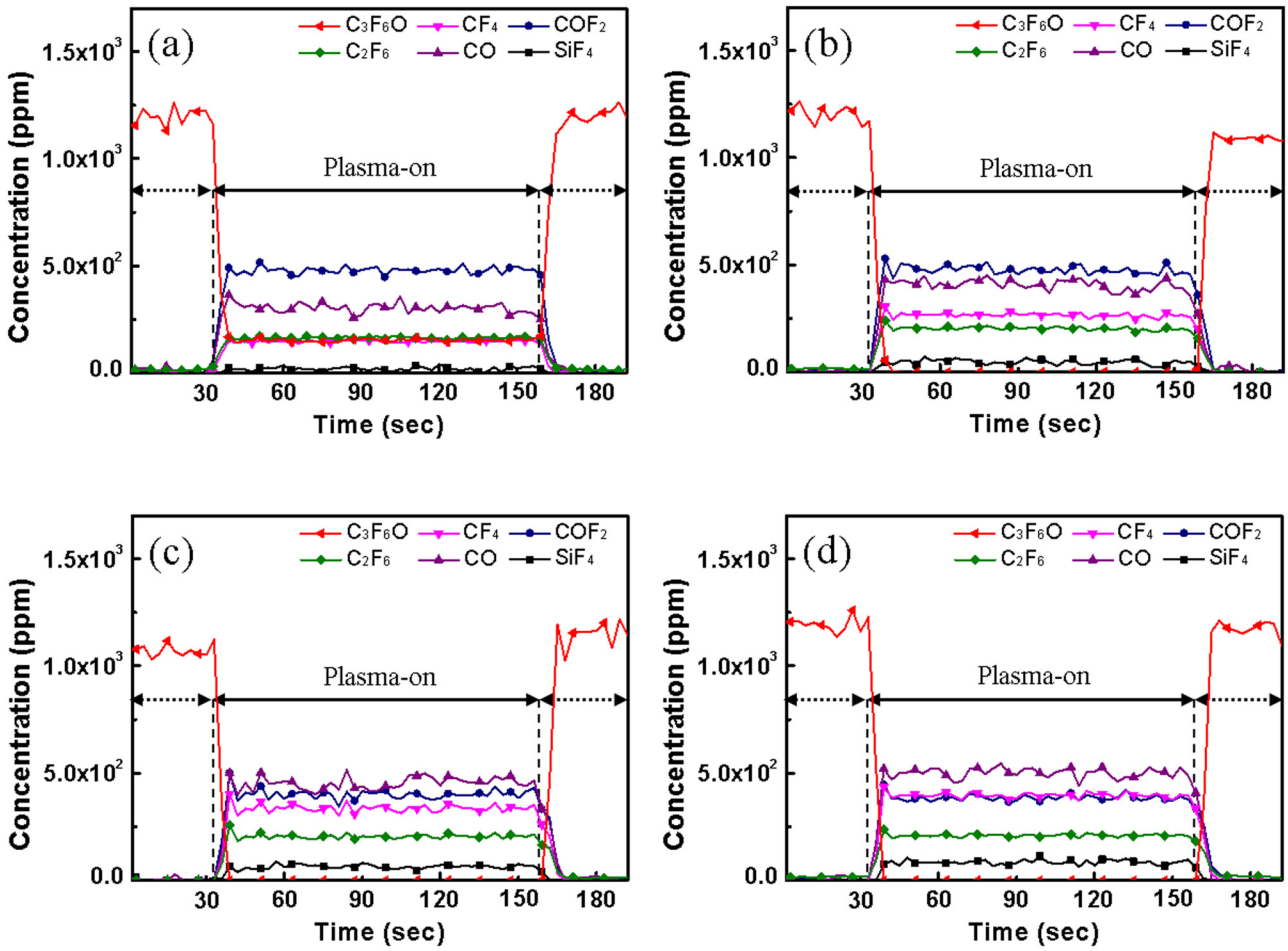

FIG. 7. Concentration of chemical species measured via FT-IR at the exhaust line during SiO_2 etching using Ar/C_3F_6O for the various rf source powers (a) 100, (b) 200, (c) 300, and (d) 400 W [Fig. 2(a)]. FT-IR measurements were carried out for 1 min before plasma-on, during plasma-on for 2 min, and for 1 min after plasma-on. An rf bias power of 2 MHz was maintained at −1100 V.

(originating from the dissociation of C_3F_6O), and of SiF_4 (by-product of the SiO_2 etch). The increased SiF_4 concentration is related to the increased SiO_2 etch rate at the higher rf source power. The concentration of COF_2, which is an intermediate C_3F_6O dissociated species and also possibly a result of a reaction with CO and F, decreased with increasing rf source power. This decrease in concentration is owing possibly to the further dissociation of COF_2.

From the above FT-IR data, the global warming effect of Ar/C_3F_6O during the etching of SiO_2 (i.e., 2 min plasma-on duration) was estimated using MMTCE, where the results are shown in Table III for the conditions specified in Figs. 7(a)–7(d). From the estimation of the global warming potential (GWP_{100}) of each emitted species, 99% of the MMTCEs were from C_2F_6 and CF_4, signifying that these were the most significant emitted species to cause global warming.

TABLE III. MMTCE values measured as a function of 2 MHz rf bias power. (a) f_{HF} (60 MHz, 100 W)/f_{LF} (2 MHz, −1100 V), Ar/C_3F_6O = 150/50 sccm, 30 mTorr. (b) f_{HF} (60 MHz, 200 W)/f_{LF} (2 MHz, −1100 V), Ar/C_3F_6O = 150/50 sccm, 30 mTorr. (c) f_{HF} (60 MHz, 300 W)/f_{LF} (2 MHz, −1100 V), Ar/C_3F_6O = 150/50 sccm, 30 mTorr. (d) f_{HF} (60 MHz, 400 W)/f_{LF} (2 MHz, −1100 V), Ar/C_3F_6O = 150/50 sccm, 30 mTorr.

Gas	Molecular weight (g/mol)	GWP_{100}	MMTCEs (a)	(b)	(c)	(d)
C_3F_6O	166.0219	100	1.31×10^{-10}	2.18×10^{-11}	1.40×10^{-11}	1.53×10^{-11}
C_2F_6	138.01	9200	9.31×10^{-9}	1.14×10^{-8}	1.16×10^{-8}	1.18×10^{-8}
CF_4	88.0043	6500	3.72×10^{-9}	6.71×10^{-9}	8.52×10^{-9}	1.00×10^{-8}
CO	28.0101	3	1.14×10^{-12}	1.49×10^{-12}	1.68×10^{-12}	1.85×10^{-12}
COF_2	66.0069	1	1.41×10^{-12}	1.39×10^{-12}	1.18×10^{-12}	1.13×10^{-12}
	Total MMTCE		1.32×10^{-8}	1.82×10^{-8}	2.02×10^{-8}	2.19×10^{-8}

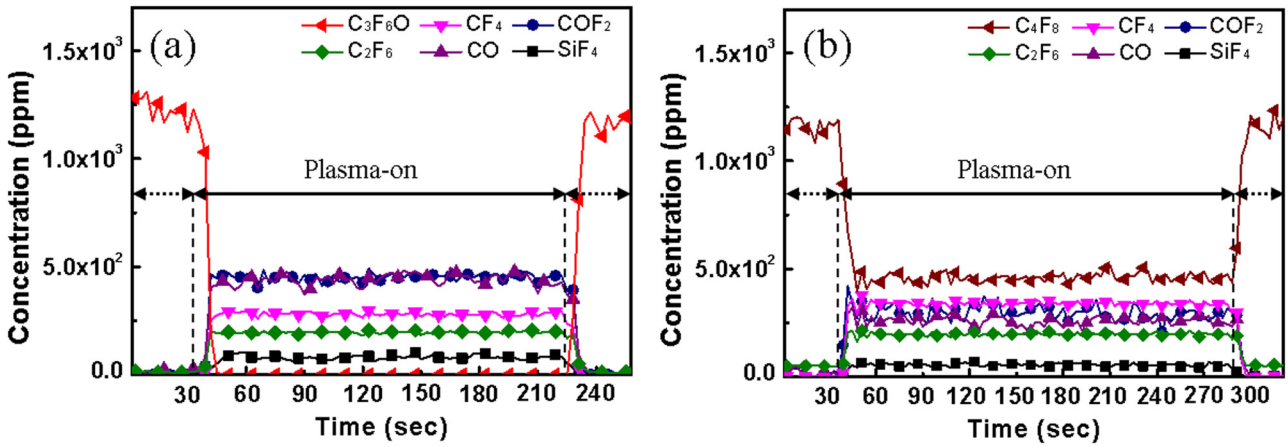

FIG. 8. Concentration of chemical species measured via FT-IR at the exhaust line during SiO_2 etching with the optimized etch conditions for Ar/C_3F_6O and $Ar/C_4F_8/O_2$, respectively, given in Figs. 5(a) and 5(b). The 60 MHz rf source power was 200 W, and the 2 MHz rf bias power was −1700 V. The plasma-on time was controlled to obtain an SiO_2 etch depth of 1 μm (3 min for Ar/C_3F_6O and 4 min for $Ar/C_4F_8/O_2$).

Contrarily, owing to the low GWPs of CO, COF_2, and C_3F_6O, the MMTCE from these species was less than 1%. In addition, a significant C_3F_6O concentration existed during the plasma-off time as well as before and after the plasma-on time. However, owing to the low GWP of C_3F_6O, the global warming effect is also very low.

For the optimized etch conditions of Ar/C_3F_6O and $Ar/C_4F_8/O_2$ specified in Figs. 5(a) and 5(b), the volumetric concentrations of the chemical species emitted after SiO_2 etching were also measured using FT-IR (Fig. 8) and their MMTCEs were calculated (Table IV). As shown in Fig. 8(a) for Ar/C_3F_6O and Fig. 8(b) for $Ar/C_4F_8/O_2$, all of the C_3F_6O was dissociated during the plasma-on duration in the former and a certain amount of C_4F_8 remained in the latter. The species with the highest volumetric concentration in the emitted gas were CO and COF_2 for Ar/C_3F_6O, owing to the significant dissociation of C_3F_6O; and C_4F_8 and CF_4 for $Ar/C_4F_8/O_2$ owing to the lesser dissociation thereof.

When the MMTCE values were compared, as shown in Table IV, the MMTCE of Ar/C_3F_6O was about 24% that of $Ar/C_4F_8/O_2$ during the plasma-on time for etching a 1 μm depth in SiO_2 (3 min for Ar/C_3F_6O and 4 min for $Ar/C_4F_8/O_2$). If the plasma-off time (1 min before plasma-on and 1 min after plasma-on) is included, the MMTCE of Ar/C_3F_6O was about 17% that of $Ar/C_4F_8/O_2$ (not shown) owing to the high GWP for C_4F_8.

TABLE IV. MMTCE values for the Ar/C_3F_6O and $Ar/C_4F_8/O_2$ chemistries. (a) f_{HF} (60 MHz, 200 W)/f_{LF} (2 MHz, −1700 V), Ar/C_3F_6O = 150/50 sccm, 30 mTorr. (b) f_{HF} (60 MHz, 200 W)/f_{LF} (2 MHz, −1700 V), $Ar/C_4F_8/O_2$ = 150/50/10 sccm, 30 mTorr.

Gas	Molecular weight (g)	GWP_{100}	MMTCEs (a)	MMTCEs (b)
C_3F_6O	166.0219	100	2.26×10^{-11}	0
C_2F_6	138.01	9200	1.67×10^{-8}	2.26×10^{-8}
CF_4	88.0043	6500	1.06×10^{-8}	1.74×10^{-8}
CO	28.0101	3	2.47×10^{-12}	1.97×10^{-12}
COF_2	66.0069	1	2.00×10^{-12}	1.78×10^{-12}
C_4F_8	200.03	8700	0	7.44×10^{-8}
Total MMTCE			2.73×10^{-8}	1.14×10^{-7}

Therefore, by using Ar/C_3F_6O instead of $Ar/C_4F_8/O_2$, a significant improvement in environmental impact can be achieved while maintaining acceptable SiO_2 etch characteristics.

IV. CONCLUSIONS

The SiO_2 etch characteristics and global warming effects of Ar/C_3F_6O gas chemistry were compared to those of the $Ar/C_4F_8/O_2$ chemistry using a DF-CCP etch system while varying the 60 MHz rf source power and the 2 MHz rf bias power. For similar rf source power and rf bias power conditions, the SiO_2 etch rates were generally higher for Ar/C_3F_6O than for $Ar/C_4F_8/O_2$, whereas the etch selectivity over the ACL was generally lower for Ar/C_3F_6O than for $Ar/C_4F_8/O_2$. This difference in etch selectivity is owing to the higher F/CF_x present in the plasma and the lower fluorocarbon layer thickness on the etched SiO_2 surface when using Ar/C_3F_6O because of the greater dissociation of C_3F_6O than of C_4F_8 under similar conditions. At the optimized etch conditions of 200 W rf source power and −1700 V rf bias voltage, the etch profile of SiO_2 with Ar (150 sccm)/C_3F_6O (50 sccm) was more anisotropic compared to that with Ar (150 sccm)/C_4F_8 (50 sccm)/O_2 (10 sccm) owing to suppression of bowing, narrowing, and necking. In these optimized conditions, Ar/C_3F_6O exhibited a much lower MMTCE value that was <24% that of $Ar/C_4F_8/O_2$, indicating a much lower global warming effect. Therefore, the C_3F_6O chemistry can be a potential replacement for the C_4F_8/O_2 chemistry because of the superior SiO_2 etch characteristics of Ar/C_3F_6O compared to those of $Ar/C_4F_8/O_2$, as well as its reduced global warming effects.

ACKNOWLEDGMENTS

This research work was supported by the Korea Institute of Energy Technology Evaluation and Planning (KETEP)

and the Ministry of Trade, Industry & Energy (MOTIE) of the Republic of Korea (No. 20172010105910).

[1]R. F. Pease and S. Y. Chou, Proc. IEEE **96**, 248 (2008).
[2]K. Kim and G. Jeong, *IEEE International Electron Device Meeting*, Washington, DC, 10–12 December 2007 (IEEE, Washington, DC, 2007).
[3]N. H. Kim, M. H. Jeon, T. H. Kim, and G. Y. Yeom, J. Nanosci. Nanotechnol. **15**, 8667 (2015).
[4]S. C. Park, S. H. Lim, C. H. Shin, G. J. Min, C. J. Kang, H. K. Cho, and J. T. Moon, Thin Solid Films **515**, 4923 (2007).
[5]S. H. Choi, J. J. Vegh, and K. K. Chi, U.S. patent 9,484,215 (6 October 2016).
[6]H. Abe, M. Yoneda, and N. Fujiwara, Jpn. J. Appl. Phys. **47**, 1435 (2008).
[7]D. B. Graves, IEEE Trans. Plasma Sci. **22**, 31 (1994).
[8]J. C. Arnold and H. H. Sawin, J. Appl. Phys. **70**, 5314 (1991).
[9]T. Nozawa, T. Kinoshita, T. Nishizuka, A. Narai, T. Inoue, and A. Nakaue, Jpn. J. Appl. Phys. **34**, 2107 (1995).
[10]N. Fujiwara, S. Ogino, T. Maruyama, and M. Yoneda, Plasma Sources Sci. Technol. **5**, 126 (1996).
[11]M. Miyake, N. Negishi, M. Izawa, K. Yokogawa, M. Oyama, and T. Kanekiyo, Jpn. J. Appl. Phys. **48**, 08HE01 (2009).
[12]M. Izawa, N. Negishi, K. Yokogawa, and Y. Momonoi, Jpn. J. Appl. Phys. **46**, 7870 (2007).
[13]K. C. Yang, S. W. Park, and G. Y. Yeom, Sci. Adv. Mater. **8**, 2253 (2016).
[14]D. Zhang and M. J. Kushner, J. Vac. Sci. Technol. A **19**, 524 (2001).
[15]W. T. Tsai, H. P. Chen, and W. Y. Hsien, J. Loss Prev. Process Ind. **15**, 65 (2002).
[16]Y. Miyawaki *et al.*, J. Appl. Phys. **52**, 016201 (2013).
[17]J. W. Butterbaugh, D. C. Gray, and H. H. Sawin, J. Vac. Sci. Technol. B **9**, 1461 (1991).
[18]C. C. Allgood, J. Fluorine Chem. **122**, 105 (2003).
[19]T. E. F. M. Standaert, M. Schaepkens, N. R. Rueger, P. G. M. Sebel, and G. S. Oehrlein, J. Vac. Sci. Technol. A **16**, 239 (1998).
[20]M. H. Jeon, A. K. Mishra, S. K. Kang, K. N. Kim, I. J. Kim, S. B. Lee, T. H. Sin, and G. Y. Yeom, Curr. Appl. Phys. **13**, 1830 (2013).
[21]D. Betowski, C. Bevington, and T. C. Allison, Environ. Sci. Technol. **50**, 790 (2016).
[22]T. R. Karl and K. E. Trenberth, Science **302**, 1719 (2003).
[23]S. Nakamura, M. Itano, H. Aoyama, K. Shibahara, S. Yokoyama, and M. Hirose, Jpn. J. Appl. Phys. **42**, 5759 (2003).
[24]UNFCCC, C.F., 2015, Adoption of the Paris Agreement.
[25]E. L. Schipper, RECIEL **15**, 82 (2006).
[26]J. P. Chang and J. W. Coburn, J. Vac. Sci. Technol. A **21**, S145 (2003).
[27]I. Namose, IEEE Trans. Semicond. Manuf. **16**, 429 (2003).
[28]F. Fracassi, R. D'Agostino, A. Fornelli, and T. Shirafuji, Jpn. J. Appl. Phys. **41**, 6287 (2002).
[29]S. H. Han, H. W. Park, T. H. Kim, and D. W. Park, Clean Technol. **17**, 250 (2011).
[30]R. Chatterjee, S. Karecki, L. Pruette, and R. Reif, Proc. Electrochem. Soc. **99**, 251 (1999).
[31]K. Y. Kim, H. K. Moon, N. E. Lee, B. H. Hong, and S. H. Oh, Electron. Mater. Lett. **11**, 93 (2015).
[32]M. B. Chang and J. S. Chang, Ind. Eng. Chem. Res. **45**, 4101 (2006).
[33]I. J. Kim, H. K. Moon, J. H. Lee, N. E. Lee, J. W. Jung, and S. H. Cho, Microelectron. Reliab. **52**, 2970 (2012).
[34]Y. Deng and D. Xiao, Jpn. J. Appl. Phys. **53**, 096201 (2014).
[35]R. Raju, D. Kudo, Y. Kubo, T. Inaba, and H. Shido, Jpn. J. Appl. Phys. **42**, 280 (2003).
[36]M. Ooka and S. Yokoyama, Jpn. J. Appl. Phys. **43**, 3586 (2004).
[37]J. H. Kim, J. W. Bae, C. H. Oh, K. J. Kim, N. E. Lee, and G. Y. Yeom, Jpn. J. Appl. Phys. **41**, 6570 (2002).
[38]B. S. Kwon, J. S. Kim, N.-E. Lee, and J. W. Shon, J. Electrochem. Soc. **157**, D135 (2010).
[39]D. Zhang and M. J. Kushner, "Surface reaction mechanisms in plasma etching processes," Ph.D. thesis (University of Illinois at Urbana-Champaign, 2000).